A&A 616, A62 (2018)
https://doi.org/10.1051/0004-6361/201832939

Astronomy & Astrophysics

K-shell photoabsorption and photoionization of trace elements

III. Isoelectronic sequences with electron number $19 \leq N \leq 26$*

C. Mendoza[1,**], M. A. Bautista[1], P. Palmeri[2], P. Quinet[2,3], M. C. Witthoeft[4,5], and T. R. Kallman[5]

[1] Department of Physics, Western Michigan University, 1903 W Michigan Ave., Kalamazoo, MI 49008, USA
e-mail: claudio.mendozaguardia@wmich.edu, manuel.bautista@wmich.edu
[2] Physique Atomique et Astrophysique, Université de Mons – UMONS, 20 place du Parc, 7000 Mons, Belgium
e-mail: patrick.palmeri@umons.ac.be
[3] IPNAS, Université de Liège, Campus du Sart Tilman, Bât. B15, 4000 Liège, Belgium
[4] ADNET Systems Inc., Bethesda, MD 20817, USA
[5] NASA Goddard Space Flight Center, Greenbelt, MD 20771, USA

Received 2 March 2018 / Accepted 30 June 2018

ABSTRACT

Context. This is the final report of a three-paper series on the K-shell photoabsorption and photoionization of trace elements (low cosmic abundance), namely F, Na, P, Cl, K, Sc, Ti, V, Cr, Mn, Co, Cu, and Zn. K lines and edges from such elements are observed in the X-ray spectra of supernova remnants, galaxy clusters, and accreting black holes and neutron stars, their diagnostic potential being limited by poor atomic data.
Aims. We here complete the previously reported radiative datasets with new photoabsorption and photoionization cross sections for isoelectronic sequences with electron number $19 \leq N \leq 26$. We also describe the access to and integrity and usability of the whole resulting atomic database.
Methods. Target representations were obtained with the atomic structure code AUTOSTRUCTURE. Where possible, cross sections for ground-configuration states were computed with the Breit–Pauli R-matrix method (BPRM) in either intermediate or LS coupling including damping (radiative and Auger) effects; otherwise and more generally, they were generated in the isolated-resonance approximation with AUTOSTRUCTURE.
Results. Cross sections were computed with BPRM only for the K ($N = 19$) and Ca ($N = 20$) isoelectronic sequences, the latter in LS coupling. For the remaining sequences ($21 \leq N \leq 26$), AUTOSTRUCTURE was run in LS-coupling mode taking into account damping effects. Comparisons between these two methods for K-like Zn XII and Ca-like Zn XI show that to ensure reasonable accuracy, the LS calculations must be performed taking into account the non-fine-structure relativistic corrections. The original data structures of the BPRM and AUTOSTRUCTURE output files, namely photoabsorption and total and partial photoionization cross sections, are maintained but supplemented with files detailing the target (N_T-electron system, where $N_T = N - 1$) representations and photon states (N-electron system).
Conclusions. We conclude that because of the large target size, the photoionization of ions with $N > 20$ involving inner-shell excitations rapidly leads to untractable BPRM calculations, and is then more effectively treated in the isolated resonance approximation with AUTOSTRUCTURE. This latter approximation by no means involves small calculations as Auger damping must be explicitly specified in the intricate decay routes.

Key words. atomic data – X-rays: general

1. Introduction

Our project is concerned with the computation of atomic data to improve the diagnostic capabilities of the spectral K lines and edges of chemical elements with low cosmic abundance (trace elements), namely F, Na, P, Cl, K, Sc, Ti, V, Cr, Mn, Co, Cu, and Zn. In spite of their low abundances, they are nevertheless observed in the X-ray spectra of supernova remnants, galaxy clusters, and accreting black holes and neutron stars (see, e.g., Hwang et al. 2000; Miller et al. 2006; Badenes et al. 2008; Kallman et al. 2009; Tamura et al. 2009; Ueda et al. 2009; Nobukawa et al. 2010; Park et al. 2013), from which they can be used to constrain the plasma characteristics. For this purpose, level energies, radiative and Auger widths, and fluorescence yields for K-vacancy levels in ions of the isonuclear sequences described above were computed by Palmeri et al. (2012; hereafter PQM12) with HFR (a Hartree–Fock code with relativistic corrections by Cowan 1981). Their atomic target representations were subsequently used by Palmeri et al. (2016; hereafter Paper I) and Mendoza et al. (2017; hereafter Paper II) to calculate intermediate-coupling photoabsorption and photoionization cross sections for isoelectronic sequences with electron number $N \leq 18$ with the Breit–Pauli R-matrix method (BPRM, Berrington et al. 1995). In this context, the resonance structures associated with the L and K ionization edges were studied in detail, particularly the radiative and spectator-Auger damping effects that lead to K-edge smearing (Palmeri et al. 2002).

In this final report of the project, we compute LS-coupling photoabsorption and photoionization cross sections for trace ions in isoelectronic sequences with $19 \leq N \leq 26$ with the

* Full Tables A.2–A.5 are only available at the CDS via anonymous ftp to cdsarc.u-strasbg.fr (130.79.128.5) or via http://cdsarc.u-strasbg.fr/viz-bin/qcat?J/A+A/616/A62
** Also Emeritus Research Fellow, IVIC, Caracas, Venezuela.

multi-purpose atomic structure code AUTOSTRUCTURE, assuming the isolated resonance approximation. This latter approach was adopted because BPRM has proven to be ineffective because the target sizes involved are too large. The accuracy of AUTOSTRUCTURE has previously been shown to be reasonable for this purpose (see Paper II), and is further examined here for the simpler K ($N = 19$) and Ca ($N = 20$) isoelectronic sequences.

An important part of this report is the curation aspects of the voluminous database that has been generated in this project (see Appendix A), which is to become available online from the CDS. We emphasize, however, that the datasets have been computed with different numerical methods and angular couplings, and their content and structures may thus vary nominally.

2. Numerical methods

The main task of this project is to compute photoabsorption and total and partial photoionization cross sections for ions of the isonuclear series P, Cl, K, Sc, Ti, V, Cr, Mn, Co, Cu, and Zn with electron numbers $N < Z - 1$, where Z is the atomic number identifying the sequence. As previously described in Paper I, species with $Z - 1 \leq N \leq Z$ will be treated elsewhere. Cross sections for isoelectronic sequences with $N \leq 11$ were reported in Paper I and with $12 \leq N \leq 18$ in Paper II. We discuss here the details of the computations for fourth-row ions with $19 \leq N \leq 26$.

The cross sections reported in Paper I and Paper II were carried out in intermediate coupling (IC) with the relativistic (Breit–Pauli) BPRM method, which allows the inclusion of radiative and spectator-Auger damping (Robicheaux et al. 1995; Gorczyca & Badnell 1996, 2000). The target representations listed in Table 9 of PQM12 were used, but for ions with $12 \leq N \leq 18$, levels from the 2s-hole configurations $[2s]\mu$ were additionally included. Electronic orbitals were generated in a Thomas–Fermi–Dirac statistical potential with the AUTOSTRUCTURE atomic structure code (Eissner et al. 1974; Badnell 2011).

Because large target sizes are required for species with $19 \leq N \leq 26$, especially those bearing ground configurations $3p^6 3d^m$ with $m > 2$, the BPRM approach is no longer practical. Exploratory calculations in Paper II revealed that LS cross sections could be adequately generated for such larger ions with a distorted-wave approach in the isolated-resonance approximation implemented in AUTOSTRUCTURE. Target models are still those from PQM12, but as previously shown (Paper II), they are complemented with levels from configurations of the type $[2s]\mu$. Radiative damping is taken into account by AUTOSTRUCTURE, but in contrast to BPRM, the Auger decay branches must be explicitly specified in the configuration list, which leads to lengthy calculations. The key feature of this approach is the decoupling of the photoionization and photoexcitation processes that enables the treatment of larger systems.

3. Results

For the trace elements hardly any previous multichannel photoabsorption cross sections for fourth-row ions with ground configurations $3p^6 3d^m$ exist; therefore we calculated the cross sections from the ionization threshold up to the monotonic decreasing tail beyond the K edge. We illustrate the main findings of our analysis in terms of the Zn ions. For the potassium isoelectronic sequence ($N = 19$), it is still possible, although involved, to perform a BPRM calculation in IC to compare with AUTOSTRUCTURE. This comparison is carried out in Fig. 1 for the $3p^6 3d\ ^2D_{3/2}$ ground state of Zn XII, where the BPRM data below the L edge (~103 Ryd) have been convolved for clarity with a Gaussian of width $\Delta E/E = 0.001$ (Fig. 1a). Salient spectral features in this region are the M edge (~30 Ryd) and the Lα transition array at ~82 Ryd, where resonance positions from the two numerical methods appear to agree adequately. Fig. 1b shows the near-K edge region above 720 Ryd, where the AUTOSTRUCTURE energy scale has been shifted by 0.9 Ryd to ensure resonance positional matching. This discrepancy is a direct consequence of adjusting the BPRM thresholds manually to the energy values listed in Table 9 of PQM12, a procedure that was performed throughout for all ions with electron number $N \leq 18$. The broad dip at ~737 Ryd in the AUTOSTRUCTURE curve of Fig. 1b is a numerical artifact resulting from the finite number ($n = 10$) of K-vacancy states considered, and it illustrates the difficulties of rendering properly the region just below threshold.

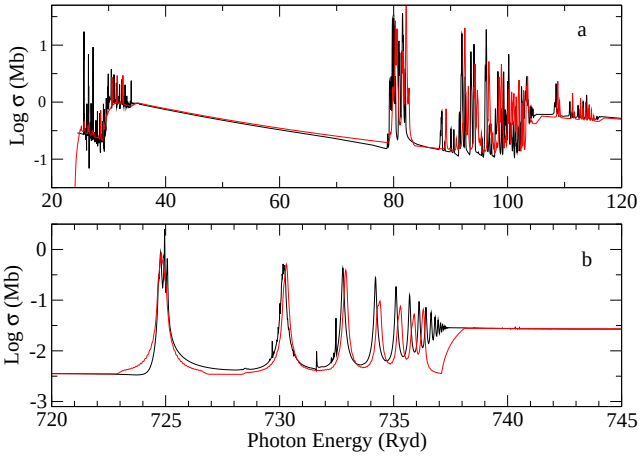

Fig. 1. IC photoabsorption cross section of the $3p^6 3d\ ^2D_{3/2}$ ground state of K-like Zn XII computed with BPRM (black curve) and AUTOSTRUCTURE (red curve). *Panel a*: valence and L-edge regions; the BPRM cross section has been convolved with a Gaussian of width $\Delta E/E = 0.001$. *Panel b*: K-edge region; the AUTOSTRUCTURE energy scale has been shifted by 0.9 Ryd to obtain resonance positional matching.

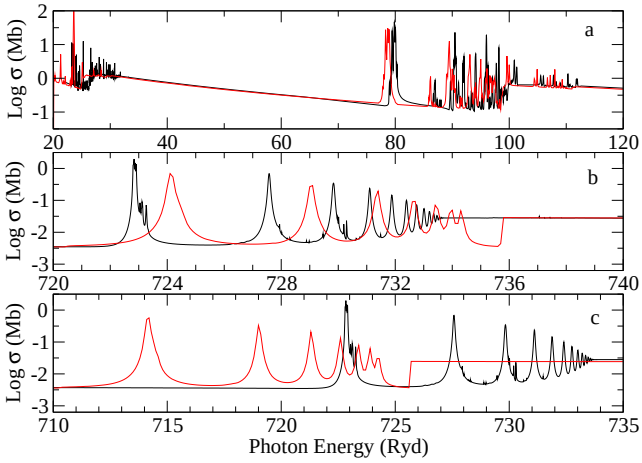

Fig. 2. *LS*-coupling photoabsorption cross section of the $3p^6 3d^2\ ^3F$ ground state of Ca-like Zn XI computed with BPRM (black curve) and AUTOSTRUCTURE (red curve). *Panel a*: valence and L-edge regions; the BPRM cross section has been convolved with a Gaussian of width $\Delta E/E = 0.001$. *Panel b*: K-edge region. *Panel c*: K-edge region where the AUTOSTRUCTURE cross section has been computed excluding the non-fine-structure relativistic corrections leading to a large positional discrepancy in the resonance structure.

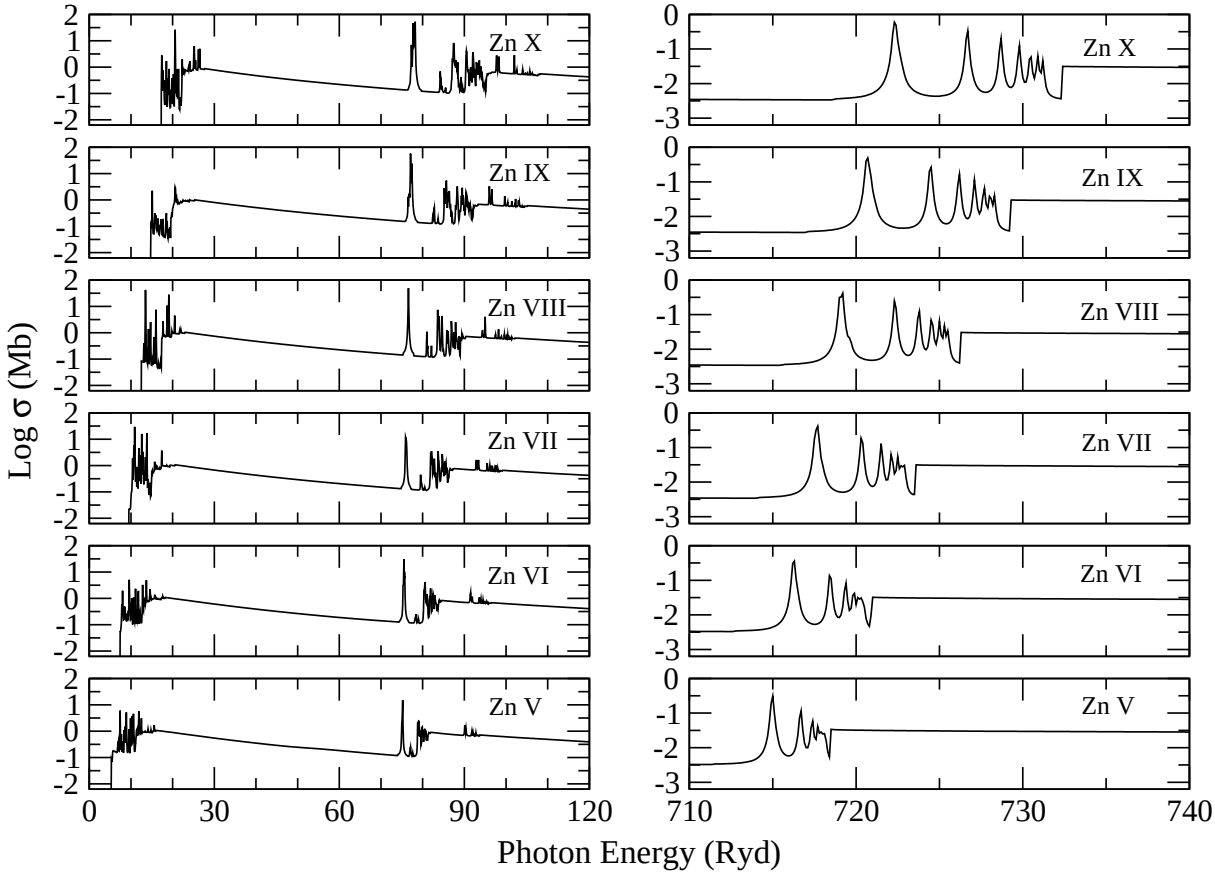

Fig. 3. AUTOSTRUCTURE *LS* photoabsorption cross sections of the ground states of Zn x (Sc-like), Zn ix (Ti-like), Zn viii (V-like), Zn vii (Cr-like), Zn vi (Mn-like), and Zn v (Fe-like) in the valence and L-edge regions (*left column*) and K-edge region (*right column*).

A similar situation is found in a comparison between BPRM and AUTOSTRUCTURE in *LS* coupling for the $3p^6 3d^2\ ^3F$ ground term of Ca-like Zn xi (Fig. 2). The positions of the AUTOSTRUCTURE L and M edges and the Lα transition array are somewhat lower (~2 Ryd) than BPRM (see Fig. 2a), while the K lines are ~1.5 Ryd higher (see Fig. 2b). Such differences are found to be typical and manageable, which is not the case if the non-fine structure relativistic corrections are neglected in AUTOSTRUCTURE, as shown in Fig. 2c, where now the discrepancies can be as large as 10 Ryd.

In Fig. 3 we plot the photoabsorption cross sections of the Zn ions of the iron-group: Zn x (Sc-like), Zn ix (Ti-like), Zn viii (V-like), Zn vii (Cr-like), Zn vi (Mn-like), and Zn v (Fe-like). The left panels show the region below 120 Ryd dominated by the L and M edges and the Lα transition arrays, while the right panels show the K edge and its associated damped lines, which are the spectral signatures of interest in X-ray astronomical spectra. An important issue here is how to improve the energy scale that is subject to the uncertainties in both the ionization potential and excitation thresholds. As shown by Gatuzz et al. (2013a,b) for the oxygen K lines, there are standing inconsistencies between the laboratory and observational energy scales that are deterrents in a reliable choice. As a consequence, no attempt is made here to adjust the energy scales.

4. Conclusions

Photoabsorption and photoionization cross sections have been computed for ions of the trace elements (elements with low cosmic abundance) F, Na, P, Cl, K, Sc, Ti, V, Cr, Mn, Co, Cu, and Zn with electron number $N \leq 26$. Cross sections were computed in intermediate coupling with the Breit–Pauli *R*-matrix method BPRM for sequences with $N \leq 20$; for the remaining sequences ($21 \leq N \leq 26$), they were obtained with AUTOSTRUCTURE in *LS* coupling because of the large target sizes, assuming the isolated resonance approximation. Comparisons between these two methods for K-like and Ca-like ions show that to ensure reasonable accuracy, it is vital to perform the *LS* calculations taking into account the non-fine-structure relativistic corrections. Curation procedures performed on the datasets stored at the CDS have been described to facilitate their download and use. These datasets will also be processed to be included in the atomic database of the XSTAR modeling code that calculates the physical conditions and emission spectra of photoionized gases (Bautista & Kallman 2001; Kallman et al. 2009).

As shown in Fig. 5b of Paper II, the BPRM photoabsorption cross section of Ar-like Sc iv in the K-edge region shows a small discontinuity at ≈331.5 Ryd where the optical potential associated with Auger damping is switched on. This feature will be found in most BPRM curves in the K-edge region. Similarly, the discontinuous AUTOSTRUCTURE cross section across the K-edge spectral head is due to the finite number of rendered resonances. This broad dip will be present in most of the cross sections computed with this code, as appreciated in Fig. 1b, Fig. 2b,c and Fig. 3 (right col.) of this report. Such numerical artifacts should be borne in mind.

There are hardly any previous calculations or experiments to reliably evaluate the accuracy of the present datasets. However, our target and collisional models have been extensively benchmarked with experiment and astronomical

observations of K-line spectra involving ionic species from cosmic abundant isonuclear series, and in some cases, assessed by independent calculations with more refined approximations (e.g., the *R*-matrix plus pseudo-states framework). More precisely, we can cite the following sequences: N (García et al. 2009; Gharaibeh et al. 2011, 2014; Sant'Anna et al. 2011; Shorman et al. 2013); O (García et al. 2005, 2011; Gatuzz et al. 2013a,b, 2014; Gorczyca et al. 2013; McLaughlin et al. 2013a,b, 2014, 2017; Bizau et al. 2015); Ne, Mg, Si, S, Ar and Ca (Palmeri et al. 2008a; Witthoeft et al. 2011b); Al (Palmeri et al. 2011; Witthoeft et al. 2013) and Ni (Palmeri et al. 2008b; Witthoeft et al. 2011a).

The L-edge structure in ions with electron number $N > 12$, as discussed in Paper II, is not expected to be fully converged in contrast to that of the K edge. Moreover, as shown by Gorczyca et al. (2013) for O I, theoretical K resonance positions are always subject to small wavelength adjustments to fit astronomical or laboratory measurements, which for this specific system have been shown to be discrepant. These data sets should therefore be treated with due caution until they are independently verified.

Acknowledgements. This project is sponsored by NASA grant 12-APRA12-0070 through the Astrophysics Research and Analysis Program. PQ and PP are Research Director and Research Associate, respectively, of the Belgian Fund for Scientific Research F.R.S.-FNRS. We are indebted to Nigel Badnell (Strathclyde University, UK) for innumerable communications regarding the possibilities, features, and switches of the AUTOSTRUCTURE computer package.

References

Badenes, C., Hughes, J. P., Cassam-Chenaï, G., & Bravo, E. 2008, ApJ, 680, 1149
Badnell, N. R. 2011, Comput. Phys. Commun., 182, 1528
Bautista, M. A., & Kallman, T. R. 2001, ApJS, 134, 139
Berrington, K. A., Eissner, W. B., & Norrington, P. H. 1995, Comput. Phys. Commun., 92, 290
Bizau, J. M., Cubaynes, D., Guilbaud, S., et al. 2015, Phys. Rev. A, 92, 023401
Cowan, R. D. 1981, The Theory of Atomic Structure and Spectra (Berkeley: University of California Press)
Eissner, W., Jones, M., & Nussbaumer, H. 1974, Comput. Phys. Commun., 8, 270
García, J., Mendoza, C., Bautista, M. A., et al. 2005, ApJS, 158, 68
García, J., Kallman, T. R., Witthoeft, M., et al. 2009, ApJS, 185, 477
García, J., Ramírez, J. M., Kallman, T. R., et al. 2011, ApJ, 731, L15
Gatuzz, E., García, J., Mendoza, C., et al. 2013a, ApJ, 778, 83
Gatuzz, E., García, J., Mendoza, C., et al. 2013b, ApJ, 768, 60
Gatuzz, E., García, J., Mendoza, C., et al. 2014, ApJ, 790, 131
Gharaibeh, M. F., Bizau, J. M., Cubaynes, D., et al. 2011, J. Phys. B At. Mol. Phys., 44, 175208
Gharaibeh, M. F., El Hassan, N., Shorman, M. M. A., et al. 2014, J. Phys. B At. Mol. Phys., 47, 065201
Gorczyca, T. W., & Badnell, N. R. 1996, J. Phys. B At. Mol. Opt. Phys., 29, L283
Gorczyca, T. W., & Badnell, N. R. 2000, J. Phys. B At. Mol. Opt. Phys., 33, 2511
Gorczyca, T. W., Bautista, M. A., Hasoglu, M. F., et al. 2013, ApJ, 779, 78
Hwang, U., Petre, R., & Hughes, J. P. 2000, ApJ, 532, 970
Kallman, T. R., Bautista, M. A., Goriely, S., et al. 2009, ApJ, 701, 865
McLaughlin, B. M., Ballance, C. P., Bowen, K. P., Gardenghi, D. J., & Stolte, W. C. 2013a, ApJ, 779, L31
McLaughlin, B. M., Ballance, C. P., Bowen, K. P., Gardenghi, D. J., & Stolte, W. C. 2013b, ApJ, 771, L8
McLaughlin, B. M., Bizau, J. M., Cubaynes, D., et al. 2014, J. Phys. B At. Mol. Phys., 47, 115201
McLaughlin, B. M., Bizau, J.-M., Cubaynes, D., et al. 2017, MNRAS, 465, 4690
Mendoza, C., Bautista, M. A., Palmeri, P., et al. 2017, A&A, 604, A63
Miller, J. M., Raymond, J., Fabian, A., et al. 2006, Nature, 441, 953
Nobukawa, M., Koyama, K., Tsuru, T. G., Ryu, S. G., & Tatischeff, V. 2010, PASJ, 62, 423
Palmeri, P., Mendoza, C., Kallman, T. R., & Bautista, M. A. 2002, ApJ, 577, L119
Palmeri, P., Quinet, P., Mendoza, C., et al. 2008a, ApJS, 177, 408
Palmeri, P., Quinet, P., Mendoza, C., et al. 2008b, ApJS, 179, 542
Palmeri, P., Quinet, P., Mendoza, C., et al. 2011, A&A, 525, A59
Palmeri, P., Quinet, P., Mendoza, C., et al. 2012, A&A, 543, A44
Palmeri, P., Quinet, P., Mendoza, C., et al. 2016, A&A, 589, A137
Park, S., Badenes, C., Mori, K., et al. 2013, ApJ, 767, L10
Robicheaux, F., Gorczyca, T. W., Pindzola, M. S., & Badnell, N. R. 1995, Phys. Rev. A, 52, 1319
Sant'Anna, M. M., Schlachter, A. S., Öhrwall, G., et al. 2011, Phys. Rev. Lett., 107, 033001
Shorman, M. M. A., Gharaibeh, M. F., Bizau, J. M., et al. 2013, J. Phys. B At. Mol. Phys., 46, 195701
Tamura, T., Maeda, Y., Mitsuda, K., et al. 2009, ApJ, 705, L62
Ueda, Y., Yamaoka, K., & Remillard, R. 2009, ApJ, 695, 888
Witthoeft, M. C., Bautista, M. A., García, J., et al. 2011a, ApJS, 196, 7
Witthoeft, M. C., García, J., Kallman, T. R., et al. 2011b, ApJS, 192, 7
Witthoeft, M. C., Bautista, M. A., García, J., et al. 2013, At. Data Nucl. Data Tables, 99, 53

Appendix A: Database content and conventions

As previously described, the datasets generated in this project are to become available online from the CDS. We give here a concise description of the adopted data conventions and structures to identify the files and facilitate the extraction of their content.

A.1. Summary

Following the close-coupling (R-matrix) convention, where a scattering system is conceived as a target plus a colliding electron, we identify the N-electron ionic species to be photoionized with the 2-tuple (Z, N_T), where Z is the atomic number and $N_T = N - 1$ is the number of target electrons. In this project we have been mainly concerned with photoabsorption and photoionization cross sections of states in the ionic ground configuration that are referred to as photon states. They are identified by the 4-tuple $(0, 2J, \pi, lev)$ in IC and $(2S+1, L, \pi, lev)$ in LS, where J and L are the total and orbital angular momentum quantum numbers, respectively, $2S+1$ the spin multiplicity, π the parity ($\pi = 0$ for even, $\pi = 1$ for odd), and lev the level index within the $J\pi/SL\pi$ series. A summary of the database content in terms of these identifiers is given in Table A.1. It may be seen therein that 24 isoelectronic sequences with target electron numbers $2 \le N_T \le 25$ have been considered encompassing elements with atomic numbers $9 \le Z \le 30$. Sequences with $N_T \ge 19$ have been treated in LS coupling, and for $N_T \ge 20$, Ni species have also been included to complement previous work by Witthoeft et al. (2011a).

Table A.1. Summary of the ionic systems studied here identified by the 2-tuple (Z, N_T), where Z is the atomic number and $N_T = N - 1$ the number of target electrons.

N_T	Z	N-electron photon states	Photon state identifiers
2	9, 11, 15, 17, 19, 21–25, 27, 29, 30	$1s^2 2s\ ^2S_{1/2}$	(0, 1, 0, 1)
3	9, 11, 15, 17, 19, 21–25, 27, 29, 30	$1s^2 2s^2\ ^1S_0$	(0, 0, 0, 1)
4	9, 11, 15, 17, 19, 21–25, 27, 29, 30	$2s^2 2p\ ^2P^o_{1/2,3/2}$	(0, 1, 1, 1), (0, 3, 1, 1)
5	9, 11, 15, 17, 19, 21–25, 27, 29, 30	$2s^2 2p^2\ ^3P_{0,1,2}, ^1D_2, ^1S_0$	(0, 0, 0, 1), (0, 2, 0, 1), (0, 4, 0, 1), (0, 4, 0, 2), (0, 0, 0, 2)
6	9, 11, 15, 17, 19, 21–25, 27, 29, 30	$2s^2 2p^3\ ^4S^o_{3/2}, ^2D^o_{3/2,5/2}, ^2P^o_{1/2,3/2}$	(0, 3, 1, 1), (0, 3, 1, 2), (0, 5, 1, 1), (0, 1, 1, 1), (0, 3, 1, 3)
7	11, 15, 17, 19, 21–25, 27, 29, 30	$2s^2 2p^4\ ^3P_{0,1,2}, ^1D_2, ^1S_0$	(0, 0, 0, 1), (0, 2, 0, 1), (0, 4, 0, 1), (0, 4, 0, 2), (0, 0, 0, 2)
8	11, 15, 17, 19, 21–25, 27, 29, 30	$2s^2 2p^5\ ^2P^o_{1/2,3/2}$	(0, 1, 1, 1), (0, 3, 1, 1)
9	15, 17, 19, 21–25, 27, 29, 30	$2s^2 2p^6\ ^1S_0$	(0, 0, 0, 1)
10	15, 17, 19, 21–25, 27, 29, 30	$2p^6 3s\ ^2S_{1/2}$	(0, 1, 0, 1)
11	15, 17, 19, 21–25, 27, 29, 30	$2p^6 3s^2\ ^1S_0$	(0, 0, 0, 1)
12	15, 17, 19, 21–25, 27, 29, 30	$3s^2 3p\ ^2P^o_{1/2,3/2}$	(0, 1, 1, 1), (0, 3, 1, 1)
13	17, 19, 21–25, 27, 29, 30	$3s^2 3p^2\ ^3P_{0,1,2}, ^1D_2, ^1S_0$	(0, 0, 0, 1), (0, 2, 0, 1), (0, 4, 0, 1), (0, 4, 0, 2), (0, 0, 0, 2)
14	17, 19, 21–25, 27, 29, 30	$3s^2 3p^3\ ^4S^o_{3/2}, ^2D^o_{3/2,5/2}, ^2P^o_{1/2,3/2}$	(0, 3, 1, 1), (0, 3, 1, 2), (0, 5, 1, 1), (0, 1, 1, 1), (0, 3, 1, 3)
15	19, 21–25, 27, 29, 30	$3s^2 3p^4\ ^3P_{0,1,2}, ^1D_2, ^1S_0$	(0, 0, 0, 1), (0, 2, 0, 1), (0, 4, 0, 1), (0, 4, 0, 2), (0, 0, 0, 2)
16	19, 21–25, 27, 29, 30	$3s^2 3p^5\ ^2P^o_{1/2,3/2}$	(0, 1, 1, 1), (0, 3, 1, 1)
17	21–25, 27, 29, 30	$3s^2 3p^6\ ^1S_0$	(0, 0, 0, 1)
18	21–25, 27, 29, 30	$3p^6 3d\ ^2D_{3/2,5/2}$	(0, 3, 0, 1), (0, 5, 0, 1)
		$3p^6 4s\ ^2S_{1/2}$	(0, 1, 0, 1)
19	22–25, 27, 29, 30	$3p^6 3d^2\ ^3F, ^3P, ^1G, ^1D, ^1S$	(3, 3, 0, 1), (3, 1, 0, 1), (1, 4, 0, 1), (1, 2, 0, 1), (1, 0, 0, 1)
		$3p^6 3d4s\ ^3D, ^1D$	(3, 2, 0, 1), (1, 2, 0, 2)
20	23–25, 27–30	$3p^6 3d^3\ ^4F, ^4P, ^2H, ^2G$	(4, 3, 0, 1), (4, 1, 0, 1), (2, 5, 0, 1), (2, 4, 0, 1)
		$3p^6 3d^3\ ^2F, ^2D2, ^2D1, ^2P$	(2, 3, 0, 1), (2, 2, 0, 1), (2, 2, 0, 2), (2, 1, 0, 1)
21	24, 25, 27–30	$3p^6 3d^4\ ^5D, ^3H, ^3G, ^3F2$	(5, 2, 0, 1), (3, 5, 0, 1), (3, 4, 0, 1), (3, 3, 0, 1)
		$3p^6 3d^4\ ^3D, ^3F1, ^3P2, ^3P1$	(3, 2, 0, 1), (3, 3, 0, 2), (3, 1, 0, 1), (3, 1, 0, 2)
		$3p^6 3d^4\ ^1I, ^1G2, ^1G1, ^1F$	(1, 6, 0, 1), (1, 4, 0, 1), (1, 4, 0, 2), (1, 3, 0, 1)
		$3p^6 3d^4\ ^1D2, ^1D1, ^1S2, ^1S1$	(1, 2, 0, 1), (1, 2, 0, 2), (1, 0, 0, 1), (1, 0, 0, 2)
22	25, 27–30	$3p^6 3d^5\ ^6S, ^4G, ^4F, ^4D$	(6, 0, 0, 1), (4, 4, 0, 1), (4, 3, 0, 1), (4, 2, 0, 1)
		$3p^6 3d^5\ ^4P, ^2I, ^2H, ^2G2$	(4, 1, 0, 1), (2, 6, 0, 1), (2, 5, 0, 1), (2, 4, 0, 1)
		$3p^6 3d^5\ ^2G1, ^2F2, ^2F1, ^2D3$	(2, 4, 0, 2), (2, 3, 0, 1), (2, 3, 0, 2), (2, 2, 0, 1)
		$3p^6 3d^5\ ^2D2, ^2D1, ^2P, ^2S$	(2, 2, 0, 2), (2, 2, 0, 3), (2, 1, 0, 1), (2, 0, 0, 1)
23	27–30	$3p^6 3d^6\ ^5D, ^3H, ^3G, ^3F2$	(5, 2, 0, 1), (3, 5, 0, 1), (3, 4, 0, 1), (3, 3, 0, 1)
		$3p^6 3d^6\ ^3F1, ^3D, ^3P2, ^3P1$	(3, 3, 0, 2), (3, 2, 0, 1), (3, 1, 0, 1), (3, 1, 0, 2)
		$3p^6 3d^6\ ^1I, ^1G2, ^1G1, ^1F$	(1, 6, 0, 1), (1, 4, 0, 1), (1, 4, 0, 2), (1, 3, 0, 1)
		$3p^6 3d^6\ ^1D2, ^1S2, ^1D1, ^1S1$	(1, 2, 0, 1), (1, 0, 0, 1), (1, 2, 0, 2), (1, 0, 0, 2)
24	27–30	$3p^6 3d^7\ ^4F, ^4P, ^2G, ^2H$	(4, 3, 0, 1), (4, 1, 0, 1), (2, 4, 0, 1), (2, 5, 0, 1)
		$3p^6 3d^7\ ^2F, ^2D2, ^2D1, ^2P$	(2, 3, 0, 1), (2, 2, 0, 1), (2, 2, 0, 2), (2, 1, 0, 1)
25	28–30	$3p^6 3d^8\ ^3F, ^3P, ^1G, ^1D, ^1S$	(3, 3, 0, 1), (3, 1, 0, 1), (1, 4, 0, 1), (1, 2, 0, 1), (1, 0, 0, 1)

Notes. Photon states of the N-electron systems for which cross sections have been calculated are identified with the 4-tuple $(0, 2J, \pi, elev)$ in IC and $(2S+1, L, \pi, elev)$ in LS. Isoelectronic sequences with $2 \le N_T \le 18$ were treated in IC and those with $19 \le N_T \le 25$ in LS.

Table A.2. IC energy-level data for target ions (Z, N_T) with $N_T \leq 18$.

Z	N_T	i	$2S+1$	L	Pi	$2J$	Conf	Term	E (Ryd)
9	2	1	1	0	0	0	1s2	1s	−151.119419
9	2	2	3	0	0	2	1s.2s	3s	53.127234
9	2	3	3	1	1	0	1s.2p	3p	53.770224
9	2	4	3	1	1	2	1s.2p	3p	53.771590
9	2	5	3	1	1	4	1s.2p	3p	53.780248
9	2	6	1	0	0	0	1s.2s	1s	53.793005
9	2	7	1	1	1	2	1s.2p	1p	54.219478
11	2	1	1	0	0	0	1s2	1s	−228.813549
11	2	2	3	0	0	2	1s.2s	3s	81.425070
11	2	3	3	1	1	0	1s.2p	3p	82.218026
11	2	4	3	1	1	2	1s.2p	3p	82.222792
11	2	5	3	1	1	4	1s.2p	3p	82.244728
11	2	6	1	0	0	0	1s.2s	1s	82.269384
11	2	7	1	1	1	2	1s.2p	1p	82.822648

Notes. The listed ground-state energy is the total ion energy, while for the remaining levels, the level energy relative to the ground state is tabulated. A complete version of this table is available at the CDS.

A.2. Target data

IC energy-level data for (Z, N_T) targets in isoelectronic sequences with $2 \leq N_T \leq 18$ and *LS* energy-level data for those with $19 \leq N_T \leq 25$ are listed in Tables A.2 and A.3, respectively. Energies in Rydbergs are given relative to the ground state, the latter listing the total ion energy. Table A.2 is very similar to Table 9 of PQM12, but since it is generated by BPRM-STG3, the level order may vary; moreover, for sequences with $N_T > 10$, the level number is greater since additional configurations were taken into account. Tables A.2–A.3 are essential when considering the partial photoionization cross sections, which for a specific N-electron photon state are tabulated in i order.

A.3. Photon-state data

The N-electron photon states for which cross sections have been computed are listed in Table A.4 (isoelectronic sequences with $3 \leq N \leq 19$ in IC) and Table A.5 (sequences with $20 \leq N \leq 26$, in *LS*); they essentially correspond to states within the ionic ground configuration. Energies are given in Rydbergs relative to the ionization potential. In systems with several photon states, IC cross sections for ions with $N \leq 19$ are tabulated in i order.

A.4. Photoabsorption and photoionization cross sections

Cross sections have been computed using the serial version of the Breit–Pauli R-matrix codes for isoelectronic sequences with target electron numbers $N_T \leq 19$ and with AUTOSTRUCTURE for $20 \leq N_T \leq 25$ (see Table A.1). Since the output files produced by these two suites of codes are somewhat different, we have

Table A.3. *LS* energy-level data for target ions (Z, N_T) with $19 \leq N_T \leq 25$.

Z	N_T	i	$2S+1$	L	Pi	Conf	Term	E (Ryd)
22	19	1	2	2	0	3p6.3d	2d	−1701.498049
22	19	2	2	0	0	3p6.4s	2s	0.600370
22	19	3	4	2	1	[3p]3d2	4d	2.268570
22	19	4	4	4	1	[3p]3d2	4g	2.414790
22	19	5	4	1	1	[3p]3d2	4p	2.425060
22	19	6	4	3	1	[3p]3d2	4f	2.503180
22	19	7	2	2	1	[3p]3d2	2d	2.523360
22	19	8	2	3	1	[3p]3d2	2f	2.537130
22	19	9	2	1	1	[3p]3d2	2p	2.591330
22	19	10	2	5	1	[3p]3d2	2h	2.640820
22	19	11	2	4	1	[3p]3d2	2g	2.660690
22	19	12	2	3	1	[3p]3d2	2f	2.668140
22	19	13	4	2	1	[3p]3d2	4d	2.725970
22	19	14	2	2	1	[3p]3d2	2d	2.858760
22	19	15	4	0	1	[3p]3d2	4s	2.889300
22	19	16	2	0	1	[3p]3d2	2s	2.889300
22	19	17	2	4	1	[3p]3d2	2g	2.904600
22	19	18	4	1	1	[3p]3d.4s	4p	3.045990
22	19	19	2	1	1	[3p]3d2	2p	3.059990
22	19	20	2	1	1	[3p]3d.4s	2p	3.119540
22	19	21	4	3	1	[3p]3d.4s	4f	3.156530

Notes. The listed ground-state energy is the total ion energy, while for the remaining levels, the level energy relative to the ground state is tabulated. A complete version of this table is available at the CDS.

kept the original nomenclature, structure, and formats rather than making an attempt to unify them. We have also avoided the conversion of cross sections computed in *LS* coupling to intermediate coupling. For an ionic species identified with the target tuple $(Z, N_T) \equiv (\mathtt{zz}, \mathtt{nn})$, the following files have been included in the database.

For isoelectronic sequences with $2 \leq N_T \leq 19$,

`zznn_xpatot`: total photoabsorption cross sections.

`zznn_xpisum`: sum of the partial photoionization cross sections. It must be noted that this sum does not take into account the Auger-damped component since it is treated in BPRM by means of a model potential that does not specify parental branching.

`zznn_xpipar`: partial photoionization cross sections.

For isoelectronic sequences with $20 \leq N_T \leq 25$,

`zznn_xpitot`: total photoabsorption cross sections.

`zznn_xdpisum`: sum of the direct partial photoionization cross sections. It must be noted that in AUTOSTRUCTURE the direct photoionization and photoexcitation processes are computed separately, and for the larger ions with $N_T > 19$, different target representations are implemented for each step that cannot be collated into a single unified target; therefore the resonance component is neglected.

`zznn_xdpipar`: direct partial photoionization cross sections.

Table A.4. IC energy-level data for photon states of (Z, N) systems for which cross sections have been computed ($N \leq 19$).

Z	N	i	0	$2J$	Pi	Lev	Conf	Term	E (Ryd)
9	3	1	0	1	0	1	1s2.2s	2s	−13.610382
11	3	1	0	1	0	1	1s2.2s	2s	−22.040222
15	3	1	0	1	0	1	1s2.2s	2s	−44.973266
17	3	1	0	1	0	1	1s2.2s	2s	−59.496210
19	3	1	0	1	0	1	1s2.2s	2s	−76.073846
21	3	1	0	1	0	1	1s2.2s	2s	−94.756868
22	3	1	0	1	0	1	1s2.2s	2s	−104.878480
23	3	1	0	1	0	1	1s2.2s	2s	−115.529476
24	3	1	0	1	0	1	1s2.2s	2s	−126.713523
25	3	1	0	1	0	1	1s2.2s	2s	−138.434645
27	3	1	0	1	0	1	1s2.2s	2s	−163.519500
29	3	1	0	1	0	1	1s2.2s	2s	−190.819322
30	3	1	0	1	0	1	1s2.2s	2s	−205.243438

Notes. Level energies are given relative to the ionization potential. A complete version of this table is available at the CDS.

Table A.5. *LS* energy-level data for photon states of the (Z, N) systems for which cross sections have been computed ($20 \leq N \leq 26$).

Z	N	i	$2S+1$	L	Pi	Lev	Conf	Term	E (Ryd)
22	20	1	3	1	0	1	3p6.3d2	3p	−2.612760
22	20	2	3	2	0	1	3p6.3d.4s	3d	−2.358835
22	20	3	3	3	0	1	3p6.3d2	3f	−2.734018
22	20	4	1	0	0	1	3p6.3d2	1s	−2.299660
22	20	5	1	2	0	1	3p6.3d2	1d	−2.629597
22	20	6	1	2	0	2	3p6.3d.4s	1d	−2.314143
22	20	7	1	4	0	1	3p6.3d2	1g	−2.585943
23	20	1	3	1	0	1	3p6.3d2	3p	−4.065680
23	20	2	3	2	0	1	3p6.3d.4s	3d	−3.298038
23	20	3	3	3	0	1	3p6.3d2	3f	−4.210251
23	20	4	1	0	0	1	3p6.3d2	1s	−3.675538
23	20	5	1	2	0	1	3p6.3d2	1d	−4.083912
23	20	6	1	2	0	2	3p6.3d.4s	1d	−3.253742
23	20	7	1	4	0	1	3p6.3d2	1g	−4.030104

Notes. Level energies are given relative to the ionization potential. A complete version of this table is available at the CDS.